2024 IEEE/RSJ International Conference on Intelligent Robots and Systems (IROS)
October 14-18, 2024. Abu Dhabi, UAE

# Improving Legged Robot Locomotion by Quantifying Morphological Computation

Vijay Chandiramani[1,2], Helmut Hauser[1,2], and Andrew T. Conn[1,2]

***Abstract*—Many robotic and biological systems exploit their morphology's interaction with the environment to become more adaptable, more energy efficient, and to simplify their control. The principles of morphological computation (MC) have been increasingly studied in recent years and researchers have investigated theoretical approaches to quantify the contribution of MC for a variety of robotic systems using only simulated models. In this work, we quantify MC in a physical robotic system, utilizing position-controlled legs with two degrees of freedom in two designs of different elastic compliance, on a bespoke test rig to execute a walking gait. The contribution of morphology was estimated by applying a theoretical model at various stages within the gait cycle to quantify the MC. The relationships between MC and the ground reaction forces and actuator energy consumption are analyzed. The results indicating that increasing the compliance in the leg morphology increases the mean MC value ($7.70 \pm 1.49$) relative to a traditional leg design ($5.03 \pm 2.27$). Periods of high MC were found to occur during the swing phase of the walking gait and reduced during the stance phase with ground reaction forces, which correlates with the findings of prior theoretical studies of MC in hopping gaits. The benefits of refining the leg morphology for higher MC is demonstrated by the measurements of cost of transport ($COT$), where the leg with the higher mean MC of 7.70 has a lower mean $COT$ of 102.8 compared to the other leg's mean $COT$ of 153.8. The results demonstrate how real-world measurements of MC may help design the morphology of improved robotics systems.**

***Index Terms*—Morphological Computation, Embodiment, Legged robots, Locomotion**

## I. Introduction

Traditionally, robotic systems are designed using rigid parts, sensors and actuators with their intended functionality being realized through feedback control systems. Active Control (AC) schemes with automated feedback loops and integrated sensors and actuators are widespread throughout robotics due to their relative ease to model and control, leveraging well-established control theory such as model linearization, adaptive control, observers, auto-tuning and others.

Although AC has been highly effective in industrial robotics, its application in open-world settings such as with legged locomotion, can be challenging [12]. This limitation largely stems from the difficulty to obtain an accurate model of the environment, since outdoor environments are inherently unpredictable. In the case of legged robots, an additional challenge is the dynamic interaction with the environments such as complex and rough terrains, which can vary dynamically under different weather conditions. Interestingly, biological systems, who are facing the same environmental challenges, have evolved different, but highly effective and efficient control approach by leveraging the dynamic properties of their body morphologies, often referred to as Morphological Computation (MC) [10] [7]. As a result, natural systems demonstrate a much better locomotion performance in unstructured environments, in comparison to any existing locomotion robots [16], [19]. It is in this context, the term morphology refers to the robot's body, explicitly including all its physical properties (shape, friction, stiffness, etc.) [10]. In the context of legged locomotion, navigating uneven terrain is possible in natural systems largely due to the physical properties of the muscle-tendon system [4] [23]. These systems not only serve a shock-absorbing role but also, within specific boundaries, can compensate for ground irregularities without the need for explicit control [18].

Researchers have therefore developed legged robots that use a blend of AC and MC in different configurations [20] by adding compliance to the body of a given robot through passively compliant elements in the body [14] or adding active compliant elements such as electro-pneumatic actuators [17], variable-stiffness mechanisms [27] and series elastic actuators [9]. Consequently, MC has played an important role in enhancing locomotion performance and simplifying control [25] [11]. To take advantage of MC fully and more systematically, it is important to find ways to measure the impact that MC has. This would allow us to optimize the design based on the robot's use-case and its proposed environment.

Therefore, in recent years, various theoretical methods to quantify MC have been proposed including by Ghazi-Zehadi et al. [5], Polani et al. [22], and Rückert and Neumann [24]. Based on review of literature thus far, the methods by Ghazi-Zehadi et al. [6] have found to be the most suitable for locomotion models. From these, 1 of the 7 models is suitable for operating on the full system's state, which enable investigation on realistic muscle models without taking approximation errors into account. In contrast, the other 6 models are based on deriving partial information from sensors and actuators and could potentially lead to errors in quantifying MC.

However, most of these studies to quantify MC have been carried out using only analytical and/or simulated models.

VC and HH are supported by grant EPSRC EP/L015293/1 and ATC is supported by EPSRC grants EP/T020792/1, EP/R02961X/1 and EP/W006235/1.

[1] School of Engineering Mathematics and Technology, University of Bristol. [2] Bristol Robotics Laboratory. Correspondence: ld19487@bristol.ac.uk

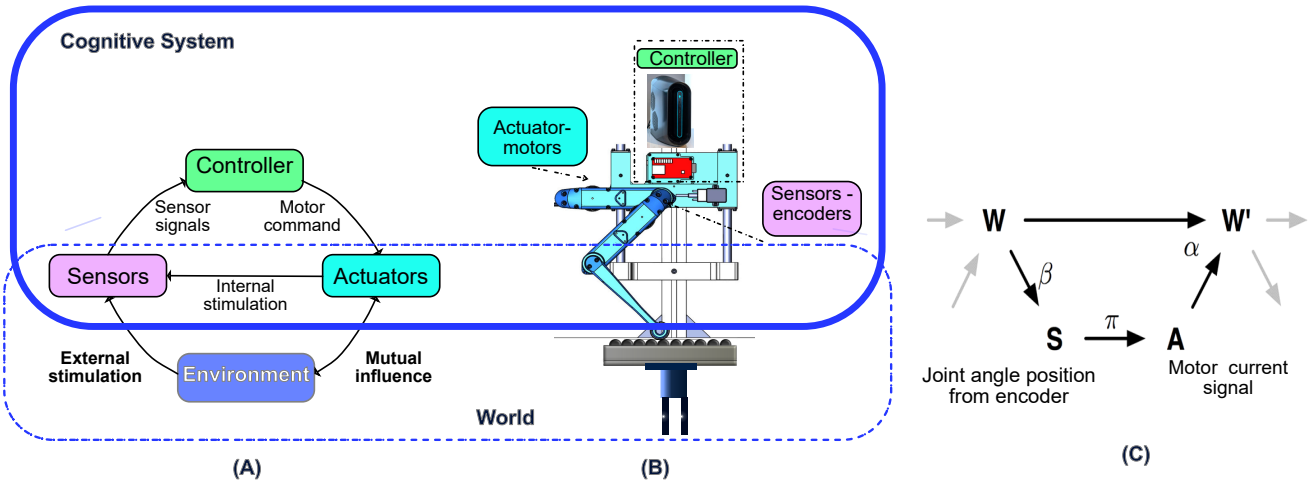


Fig. 1: (A) Sensorimotor loop (SML) displaying the information flow (B) the test rig comprising 2DoF leg landing on a passive tread-mill, mapping to the SML (C) a directed graph that illustrates the causal relationships between the world (W), Sensor (S) and Actuator (A) along with the kernels $\alpha, \beta$ and $\pi$ specifically in relation to the 2DoF leg (adapted from [6]).

Unfortunately, the limited fidelity of simulations can lead to discrepancies in the behavior of real robotic systems [15], which highlights the need to quantify MC in physical systems to help develop robots with an improved blend of AC and MC.

In this work, in contrast to prior simulation-based studies, we quantify MC in a real legged robotic system using a two segment single leg mechanism based on the design of the Open Dynamic Research Initiative (ODRI) Solo8 quadruped [8]. The bespoke design included legs with different morphologies, a passive treadmill with free rolling mechanism, and modifying the control system, as elaborated in Section III. These enhancements resulted in a flexible platform to conduct a range of experiments related to MC, leading to the following contributions: 1) Quantifying MC on a physical robot at different stages of the walking gait and its aggregated value; 2) Investigating the benefits of MC on the energy consumption and efficiency of the physical robot.

This paper is organized in three sections. In Section II, we start with a conceptual understanding of quantifying MC and the design of the 2DoF leg experimental platform. Section III describes the results where we quantify the morphological computation (MC) in the walking gait and explore the impact of various morphologies. Finally, in Section IV, we discuss the results and future work.

## II. Method

### A. Measuring Morphological Computation

For the quantification of MC we employ a theoretical approach proposed by Ghazi-Zahedi et al. [5]. It is based on a formal representation of the sensorimotor loop (SML). As shown in Figure 1, the sensorimotor loop can be considered equivalent to the common control loop used in most robotic systems [2], comprising the controller ('cognitive system'[1]), which sends signals to the actuators, thereby generating force/torque and motion to interact with the environment. To effectively model uncertainties in the environment and in the internal dynamics, random variables are employed. For the sensorimotor loop we considered two types of variables, i.e., sensor and actuator signals. As proposed in [5], both are captured as random variables to account for the noise in the measurements and uncertainties in how the robot can affect the world.

It is important to note that the body and environment are encapsulated in one single random variable named 'world' as shown in Figure 1(A). From the perspective of the 'cognitive system', the world encompasses all that is extrinsic, while the signals from controllers, sensors, and actuators are intrinsic to the system. This concept is consistent with the agent-environment separation seen in reinforcement learning [26], where the environment is defined as all aspects that the agent cannot control arbitrarily.

In this context the sensorimotor loop can be represented as three stochastic processes, $W[t]$ (world), $S[t]$ (sensing) and $A[t]$ (actuating), which are connected through three corresponding random variables at time $t$ corresponding to state of the world, $w[t]$, sensors $s[t]$, and actuators $a[t]$ respectively [5]. In the context of the 2DoF test rig we use here, see Figure 1(B), $w[t]$ is the state of the robot in a given time-step $t$, which includes its position and angular velocity. Correspondingly, the random (sensor)variable $s[t]$ represents the signals from the load-cell to measure the ground reaction force (GRF) and the encoder signals provided by measuring

[1]The definition of a 'cognitive system' has evolved over time beyond the current representation by Ghazi-Zahedi et al. [5] and will be used in this text to retain the original author's research

the joint angle positions. The actuator state $a[t]$ represents the electric current signal to the motor.

The directed edges in Figure 1(C) reflect causal dependencies between these random variables. Time is considered to be discrete, i.e., $t \in \mathbb{N}$. For the sake of simplifying the notation we write $w[t]$ as $w$ and $w[t+1]$ as $w'$.

The stochastic maps $\alpha$, $\beta$, and $\pi$, also referred to as kernels, describe the mechanisms that are involved in the sensorimotor loop dynamics. Specifically, $\beta(s|w)$ is the sensor kernel, which determines how the robot perceives the world, i.e., how the world state affects the sensory state. This means, given a world state $w \in W$, the response of the sensor is characterized by a probability distribution $\beta(s|w)$ of possible sensor states $s \in S$. The kernel $\pi(a|s)$ is the robot's controller or policy, which maps the current sensor state $s \in S$ onto an action of the robot, i.e., actuator signal $a \in A$ . In other words, this is the closed loop control system, further described in Section II (D). Finally, $\alpha(w'|w,a)$ describes the world dynamics. It represents the change of world state from $w$ to $w'$ (i.e., from one time step to the next) when a certain action $a$ is applied. The kernels $\alpha$ and $\beta$ are extrinsic and encode the constraints of the sensorimotor loop due to the robot's morphology and the properties of the environment. The kernel $\pi$ is intrinsic with respect to the robot and can be modified.

Having described the sensorimotor loop, we can now proceed to derive the mathematical formulation for quantifying MC. To facilitate a better understanding, let's consider special situations. For examples, let's assume the state of the world at any given time step $t$ has no impact on its state at the subsequent time step. In other words, within the diagram depicted in Figure 1(C), there is an absence of a causal connection between $w$ and $w'$. Under these circumstances, the state of the robot is fully determined by the actions of the controller, which implies that MC does not occur, [5]. It follows that in the case of absence of MC, the world dynamics kernel $\alpha(w'|w,a)$ would reduce to $p(w'|a)$, since there is no influence of the previous world state $w$. Any deviation from this controller-dependent behavior indicates that the previous world state $w$, had an impact. Consequently, information about $w$ alters the probability distribution over the subsequent world state $w'$. The difference between the two distributions, $\alpha(w'|w,a)$ and $p(w'|a)$ stem from the system's behavior being affected by passive control within the system. This difference is measured using the Kullback-Leibler divergence $D_{KL}(\alpha(w'|w,a)||p(w'|a))$ [5]. It is computed as:

$$MC = \sum_{w',w,a} p(w',w,a) log_2 \frac{\alpha(w'|w,a)}{p(w'|a)}. \quad (1)$$

Equation 1 shows that this measure can be computed from observations of $w$, $a$, and $w'$ alone, i.e., the evolving state of the world ($w \rightarrow w'$) and the actuation $a$. As mentioned before, $a$ is the electrical current signal to the motor measured over time (i.e., as a time series). Similarly, $w$ is the univariate variable combined from the Cartesian position of the foot in the $z$-axis and the angular velocity of the knee, both measured over time. We measure the position only in the $z$-axis because the interactions of the leg with the environment (passive treadmill) happens in this direction in the walking gait cycle [6]. The $x$-axis is simply to measure the stride length.

Therefore, in the context of the 2DoF leg in this work, the MC can be computed by using $N$ time steps collected from the variables that are required for the world and the actions. For the world $w$, we require two variables, the Cartesian vertical leg position relative to the robot's foot over time, $C_z(t) = (C_z(1), C_z(2), \ldots, C_z(N))$ and angular velocity of the knee over time, $\omega_2(t) = (\omega_2(1), \omega_2(2), \ldots, \omega_2(N))$. For the controller output over time $a$, we require the electrical current signal to the motor $i(t) = (i(1), i(2), \ldots, i(N))$. After these signals are logged, they need to be pre-processed into discretized data, by binning this continuous data into a smaller number of bins. Taking the example of the electrical current signal, with $B = 100$ bins (the approach to selection of number of bins is beyond the scope of this paper) the discrete electrical current is $i[t] = ((i(t) - min(i(t))/((max(i) - min(i)) * B$. Similarly, the other variables $C_z$, $\omega_2$ and $i$ are discretized. The next step is to create the univariate variable $w$ by combining $C_z$ and $\omega$. The objective of creating a univariate variable is to simplify data analysis. Creating a univariate variable from multiple discrete variables involves combining or transforming these variables into a single variable using a suitable combination logic based on the objective. In case of this robot, a custom function is used: $w = C_z[t] + H * \omega[t]$, where $H$ is the scaling factor that is sufficiently large to balance the contribution of $\omega[t]$.

Having calculated $a$ and $w$, the next step is to compute the joint probability distribution $p(w', w, a)$ as follows:

$$p(w', w, a) = \frac{\text{number of occurrences}(w', w, a)}{\text{total number of observations}} \quad (2)$$

In the software, it is implemented as an iterative loop over time $t$. The other probabilities $p(w, a)$ and $p(a)$ are computed in a similar way. Further, both conditional probability distributions are calculated from the joint distribution in the following way [5]:

$$\alpha(w'|w,a) = \frac{p(w', w, a)}{p(w, a)} \quad (3)$$

$$p(w'|a) = \frac{p(w', w, a)}{p(a)} \quad (4)$$

In the final step, MC (Equation 1) is computed by substituting probability values obtained in Equations 3 and 4. Having defined and quantified MC in the context of a legged robot, we move on now to describe the experimental set-up.

### *B. Experimental setup: robot leg with 2 DoF*

A 2DoF single leg mechanism, based on the impedance-controlled ODRI Solo8 robot [8], was built and mounted on a bespoke test rig with a passive, low friction 1DoF linear

guide, as shown in Figure 2(A. The actual images are shown in Figure 3.

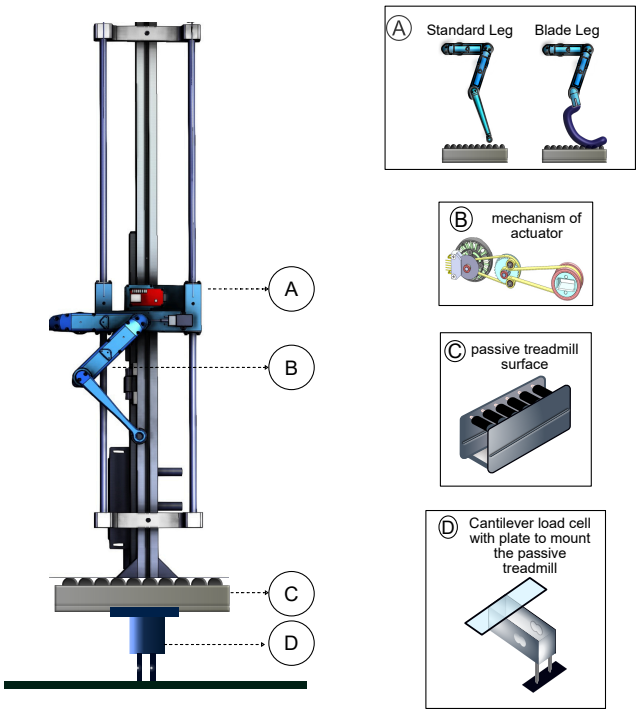


Fig. 2: 2DoF leg mounted on a test rig with (A) The 2DoF Original and Blade legs on linear guide assembly to allow vertical movement on the rails; (B) Actuator construction showing the motor, encoder and belt transmission; (C) The passive treadmill surface; (D) Cantilever load-cell to measure the GRF [21].

The leg consisted of actuated hip and knee joints that were fabricated from 3D printed ABS (on an *Ultimaker S3*) with stainless steel roller bearings for the output, belt transmission and motor shaft (*EZO MR84, 6832Z and 61705 2RS*). The hip joint was connected to a rigid structure that was mounted on two parallel stainless steel rods via linear bearings to allow for a constrained vertical motion during a selected gait. The actuator module was torque-controlled, comprising a brushless DC motor (BLDC) *(T-Motor 4004)*, a high resolution optical encoder *(Broadcom AEDT-9810-Z00)*, and a dual stage timing belt transmission *(AT3 Synchroflex 3mm pitch)* in a gear ratio of 1:9, as shown in Figure 2(B). The foot landed on a passive treadmill with free-spinning rollers (Figure 2(C)) to enable the lateral movement of the foot when in contact with the ground. Underneath the treadmill, there was a cantilever load cell *(Stemedu 1kg)* that measured the Ground Reaction Force (GRF) as shown in Figure 2(D).

### C. Elastic leg design

The standard leg configuration in the ODRI Solo8 design [8] has rigid leg segments and no elasticity in the joints. To investigate how morphological changes affect MC and impact the legged locomotion performance, we designed an elastic leg segment that was able to store more elastic energy compared to the standard design. To achieve that we replaced the lower leg segment with the curved blade structure shown in Figure 2 (A). The elastic leg segment was 3D printed using ABS, based on the design in [1].

### D. Generating the walking gait

In this section, we first describe the walking gait phases to provide a framework to analyze variations of MC throughout the gait-cycle. This is followed by the kinematics and control systems required to achieve the desired trajectory.

The 2DoF leg is a planar system moving in the $x-z$ axis, as shown in Figure 4. The walking gait comprise two main phases, (1) the stance phase and (2) the swing phase. The stance phase is the period of the gait cycle when the foot is in contact with the ground and it comprises three main sub-phases:

- The strike: the foot makes initial contact with the ground,
- Loading response: the foot rolls forward until the entire surface is in contact with the ground,
- Take-off: which generates forward propulsion and is the final contact with the ground.

In the swing phase the foot is not in contact with the ground. The corresponding sub-phases are:

- Early swing: the foot is lifted off the ground,
- Mid-swing: the leg passes beneath the body,
- Late swing: the foot moves to its highest point in its trajectory from where it is ready to move towards the strike sub-phase.

The forward kinematics are computed as shown in Figure 4(B) using:

$$C_z = l_1 cos\theta_1 + l_2 cos\theta_{12}, \tag{5}$$

$$C_x = l_1 sin\theta_1 + l_2 sin\theta_{12}, \tag{6}$$

$$\text{where, } \theta_{12} = \theta_1 + \theta_2. \tag{7}$$

Using trigonometry (not shown due to triviality), the joint angles $(\theta_1, \theta_2)$ required for the foot position in Cartesian space $(C_x, C_z)$ are:

$$\theta_2 = atan2\left( +/- \sqrt{1 - \left(\frac{C_x^2 + C_z^2 - l_1^2 - l_2^2}{2l_1 l_2}\right)^2}, \frac{C_x^2 + C_z^2 - l_1^2 - l_2^2}{2l_1 l_2}\right)$$

$$\theta_1 = atan2\left(+/- \sqrt{1 - \left(\frac{C_x(l_1 + l_2 cos\theta_2) + C_z l_2 sin\theta_2}{C_x^2 + C_z^2}\right)^2}, \frac{C_x(l_1 + l_2 cos\theta_2) + C_z l_2 sin\theta_2}{C_x^2 + C_z^2}\right) \tag{8}$$

The desired Cartesian coordinates of the foot are derived from the walking gait, and the corresponding desired joint angles

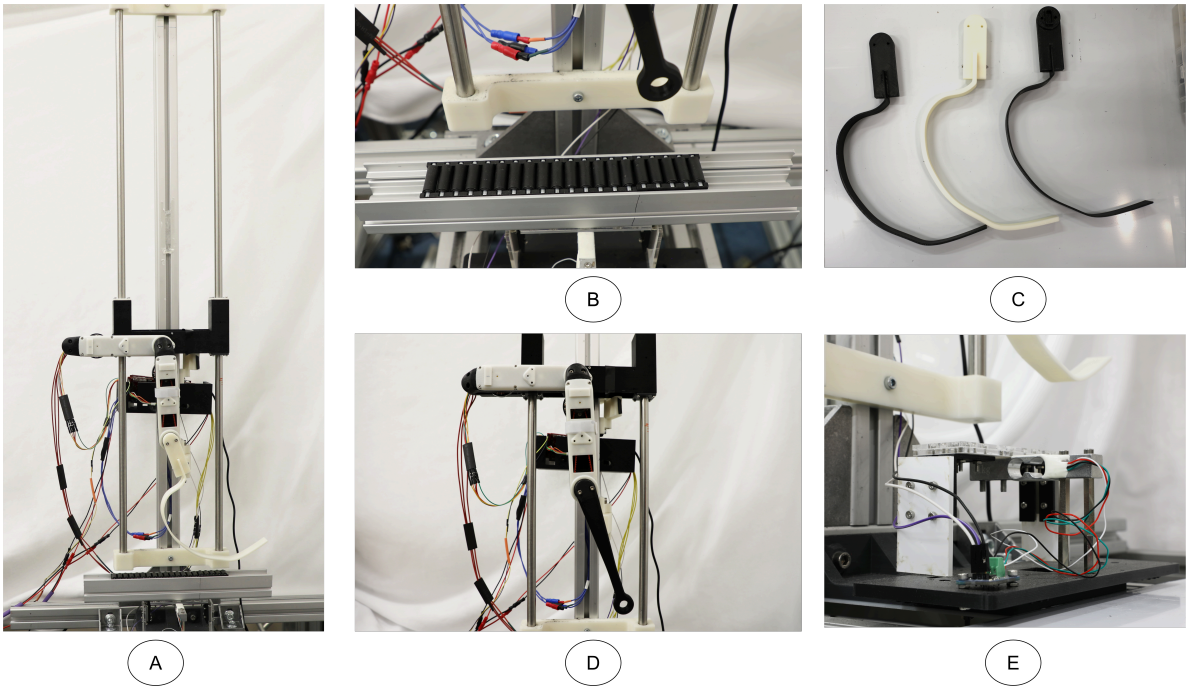


Fig. 3: Actual set-up (A) Complete test rig with 2Dof Blade leg mounted on the test rig (B) Passive tread-mill (C) Blade legs of different thicknesses (D) Close-up of the test rig with the Original leg (E) Cantilever load-cell assembly

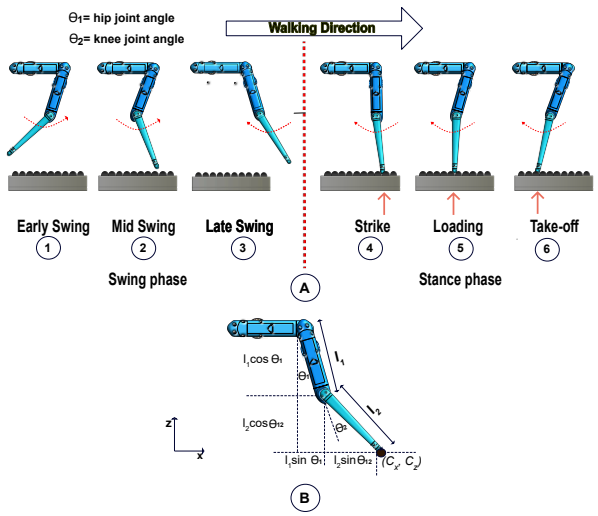


Fig. 4: (A) Walking gait cycle showing the swing (1,2,3) and stance phases (4,5,6) of the *Original-Active* leg (B) Kinematics of the 2DoF leg with Cartesian coordinates $(C_x, C_z)$ of the foot position

computed using Equations 8. For the hip and knee individually, the gait is generated using the sine wave trajectory defined as:

$$\theta[t] = \theta[t]_{ref} sin(2\pi ft + \phi), \quad (9)$$

where, $\theta[t]$ is the joint angle positions $(\theta_1, \theta_2)$ at time-step $t$, $\theta[t]_{ref}$ the desired joint angle from Equations 8, $f$ the frequency, and $\phi$ the phase shift.

As shown in Figure 5, the trajectory for each joint is achieved using a proportional differential (PD) controller with gains $K_p$ and $K_d$. The PD controller is designed to minimize the error between the desired, $\theta[t]_{ref}$, and actual, $\theta[t]_{act}$, joint angles. This is achieved by modulating the motor current, $i[t]$, which is proportional to the torque. Therefore, the inner feedback loop is defined as:

$$i[t] = K_p(\theta[t]_{ref} - \theta[t]_{act}) + K_d(\omega[t]_{ref} - \omega[t]_{act}) \quad (10)$$

where, $\omega[t]_{ref}$ and $\omega[t]_{act}$ are the desired and actual angular velocities, respectively.

During the experiments, the joint angles and motor current were recorded via a *TI Launchpad MCU* connected to the *Linux Ubuntu PC* using *Controller Area Network (CAN)* and were used to quantify MC as per Equation 1. We map the variables as follows: the actuator state $a[t]$ is the motor current $i[t]$, and the world state $w[t]$ is created as a univariate variable from leg position $C_z[t]$ and the angular velocity of the knee joint $\omega[t]$.

The outer loop joint angle position control system ran at a frequency of 1 kHz and was implemented in *C++* in the *ROS2 Humble* environment running *Linux Ubuntu 22.04*, and communicated using the *Controller Area Network*

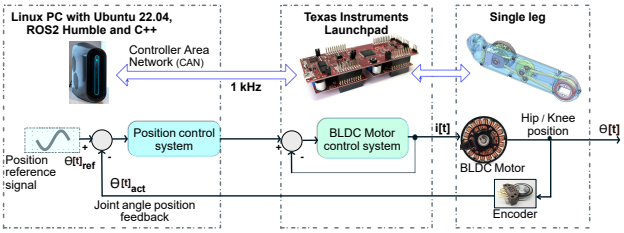


Fig. 5: Control System schematic for one motor showing the hardware and software set-up. The reference signal is the joint angle following a sinusoidal trajectory. The outer loop is a PD position control system, providing a current reference to the BLDC motor torque controller embedded in the TI Launchpad MCU.

(CAN) protocol with the *Texas Instruments* (TI) *Launchpad Microcontroller Unit* (MCU).

### *E. Experimental procedure*

The experiments were designed to investigate the impact of different leg morphologies on the contribution of MC (using Equation 1). In addition, we studied the effect of MC on the robot's energy efficiency, to evaluate whether more MC results in more energy-efficient robots. To achieve these objectives, a walking gait (Equation 9) repeated over 20 cycles was run on the two 2DoF legs:

1) *Original-Active* - Original leg with both hip and knee actuated,
2) *Blade-Active* - Blade leg with both hip and knee actuated.

MC is quantified as described in Section II. The raw value of the MC was noisy and therefore, it was smoothed using a Gaussian filter in MATLAB. Furthermore, the power consumption ($P$), the total energy consumed ($E$), and the Cost of Transport ($COT$) were computed as follows:

$$P = k_t|i_{hip}||\omega_{hip}| + k_t|i_{knee}||\omega_{knee}|, \tag{11}$$

$$E = \int_t P dt, \tag{12}$$

$$COT = \frac{E}{mgd}, \tag{13}$$

where the mass of the robot $m$ = 0.7 kg, gravitational acceleration $g$ = 9.81 $m/s^2$, torque constant $k_t$ = 0.025 Nm/A and $d$ is the distance traveled. Since the robot does not translate laterally, being constrained on the test rig, $d$ is computed by summing up the measured stride length over 20 cycles. The measured currents and angular velocities can be positive or negative due to bidirectional motor rotation. Therefore, we take their absolute values to compute the energy consumption.

## III. Results

Figure 6 shows MC and GRF being measured during walking gait for the two legs configurations, *Original-Active* and *Blade-Active*. We start by considering the quantified MC values with the *Original-Active* leg configuration.

As shown in Figure 6(A), during the early swing sub-phase (1), MC is high because the behavior of the system is governed only by the interaction of the body (mass, velocity, position) and gravity and not by the actuators. As it approaches the midswing sub-phase (2), the robot shows a decline of MC due to the fact that the actuators' relative contribution to drive the desired trajectory increases.Subsequently, MC drops as soon as the foot touches the ground (4) at the start of the stance phase, since at this point the robot needs to use a higher proportion of active control (AC) to overcome frictional forces to follow the desired trajectory. Shortly after touching the ground, during the loading phase (5), the system shows a strong decline of MC as actuation torque increases towards take-off (6), at which point there is a strong increase in MC as the swing phase starts (as described above). In the loading sub-phase (5), the ground reaction force (GRF) is at its highest value.

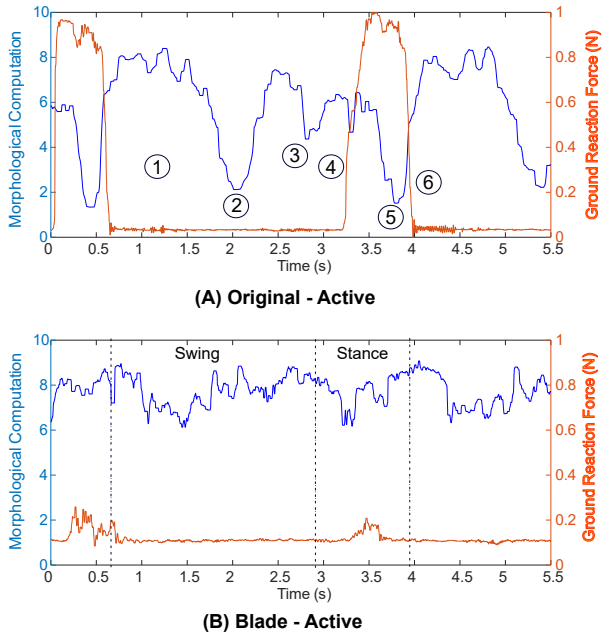


Fig. 6: Quantified experimental MC and Ground Reaction Force plotted across the different phases of the walking gait, for (A) Original-Active and (B) Blade-Active leg configurations. The sub-phases 1 to 3 (Swing) and 4 to 6 (Stance) are defined in Figure 4.

The *Blade-Active* leg shows a higher MC across the entire walking gait cycle ranging from around 6 to 9 with a mean of ($\mu = 7.70 \pm 1.49$). In comparison, the *Original-Active* leg ranges from approximately 3 to 7 ($\mu = 5.03 \pm 2.27$), which indicates that a more elastically compliant leg can help increase the MC. It can also be noted that the *Blade-Active* leg has a peak GRF in the loading and mid-stance phases of approximately $0.25N$, as compared to $1N$ in the *Original-Active* leg (Figure 6). This is primarily due to the

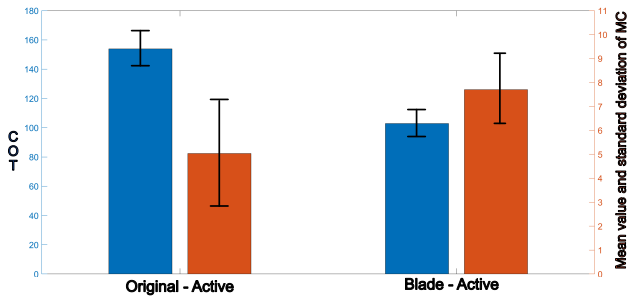


Fig. 7: Mean Cost of Transport and the Mean MC of the *Original-Active* and the *Blade-Active* leg design. The Blade shows higher energy efficiency and higher MC in comparison to the Original due to the elastic compliance offered by the Blade design.

elastic compliance provided by the blade's morphology when it comes in contact with the passive treadmill.

One potential benefit of morphological computation is to help achieve more energy efficient locomotion. Therefore, we calculate the $COT$ (Equation 13) in the two leg configurations and the results are summarized with the mean MC measurements in Figure 7. The *Original-Active* leg has a mean MC of 5.03 (s.d. $\pm$2.27) and mean $COT$ of 153.8 (s.d. $\pm$12.01), whereas the *Blade-Active* leg shows the higher mean MC of 7.70 (s.d. $\pm$1.49) and lower mean $COT$ of 102.8 (s.d. $\pm$9.08), demonstrating the best energy efficiency of the two legs. This suggests that MC can act as a useful metric to help design legs with improved energy efficiency.

## IV. Discussion

This work presented how MC can be quantified in a real robotic leg over multiple gait cycles. We further demonstrated that the robot's behavior is affected by changes in its morphology, using $COT$ as the basis for comparisons of MC and energy usage. A detailed optimization of the leg design was outside the scope of this study, but this work provides a crucial demonstration of how MC can used as a quantifiable metric with the potential to investigate different designs and optimize physical robots, by considering the effects of MC on performance proactively.

A key conclusion is that this test rig can be used to quantify MC on a real robot in a controlled indoor environment with an arbitrary gait, since the MC calculations are based on capturing time-series data representing the world and the actuator state. This can serve as a platform for experimentally verified design optimization after the simulation phase and therefore lead onto deployment in real outdoor environments. A second principal conclusion is that we demonstrate how increased MC can act as a metric for decreased $COT$, which could help expand the design space used to develop more energy efficient robots. In fact, research by Li et al. using a snake-like robot [13] and by Borisov et al. using elastic springs on a legged robot [3] demonstrates the effect of MC on energy efficiency.

Limitations in the present study that will be addressed in future work include the fact that measurements took place in a controlled indoor environment, which constrained the complexity robot-world interaction. It is planned to extend the methodology in this study to an indoor walking robot (after [8]) to quantify MC with full 6-DoF body dynamics and measure its impact on the robot's behavior. Subsequently, the robot will be tested in an outdoor environment using different terrains to quantify MC in a dynamic setting.

## References

[1] Y. Alizadeh. Design and structural analysis of composite prosthetic running blades for athletes, 2021.

[2] N. Ay and K. Zahedi. *On the Causal Structure of the Sensorimotor Loop*, pages 261–294. Springer Berlin Heidelberg, Berlin, Heidelberg, 2014.

[3] I. I. Borisov, I. A. Kulagin, A. E. Larkina, A. A. Egorov, S. A. Kolyubin, and S. Stramigioli. Study on elastic elements allocation for energy-efficient robotic cheetah leg. In *2019 IEEE/RSJ International Conference on Intelligent Robots and Systems (IROS)*, pages 1696–1701, 2019.

[4] I.E. Brown, S.H. Scott, and G.E. Loeb. Preflexes. In *Programmable, High-gain, Zero-delay Intrinsic Responses of Perturbed Musculoskeletal Systems. Soc Neurosci Abstr*, volume 21, 1995.

[5] K. Ghazi-Zahedi. *Morphological Intelligence*. Springer, 2019.

[6] K. Ghazi-Zahedi, D.F.B. Haeufle, G. Montúfar, S. Schmitt, and N. Ay. Evaluating morphological computation in muscle and dc-motor driven models of hopping movements. *Frontiers in Robotics and AI*, 3, 2016.

[7] K. Ghazi-Zahedi, J. Rieffel, S. Schmitt, and H. Hauser. Editorial: Recent trends in morphological computation. *Frontiers in Robotics and AI*, 8, 2021.

[8] F. Grimminger, A. Meduri, M. Khadiv, J. Viereck, M. Wuthrich, M. Naveau, V. Berenz, S. Heim, F. Widmaier, T. Flayols, and et al. An open torque-controlled modular robot architecture for legged locomotion research. *IEEE Robotics and Automation Letters*, 5:3650–3657, April 2020.

[9] D.W. Haldane, M.M. Plecnik, J.K. Yim, and R.S. Fearing. Robotic vertical jumping agility via series-elastic power modulation. *Science Robotics*, 1(1), 2016.

[10] H. Hauser, A.J. Ijspeert, R.M. Füchslin, R. Pfeifer, and W. Maass. Towards a theoretical foundation for morphological computation with compliant bodies. *Biological Cybernetics*, 2011.

[11] M. Hutter, C. Gehring, D. Jud, A. Lauber, C. D. Bellicoso, V. Tsounis, J. Hwangbo, K. Bodie, P. Fankhauser, M. Bloesch, R. Diethelm, S. Bachmann, A. Melzer, and M. Hoepflinger. Anymal - a highly mobile and dynamic quadrupedal robot. In *2016 IEEE/RSJ International Conference on Intelligent Robots and Systems (IROS)*, pages 38–44, 2016.

[12] N. Kottege, L. Sentis, and D. Kanoulas. Editorial: Towards real-world deployment of legged robots. *Frontiers in Robotics and AI*, 8, 2022.

[13] Longchuan Li, Shugen Ma, Isao Tokuda, Fumihiko Asano, Makoto Nokata, Yang Tian, and Liang Du. Generation of efficient rectilinear gait based on dynamic morphological computation and its theoretical analysis. *IEEE Robotics and Automation Letters*, 6(2):841–848, 2021.

[14] X. Liu, A. Rosendo, S. Ikemoto, M. Shimizu, and K. Hosoda. Robotic investigation on effect of stretch reflex and crossed inhibitory response on bipedal hopping. *Journal of The Royal Society Interface*, 15(140):20180024, 2018.

[15] S. Masuda and K. Takahashi. Sim-to-real transfer of compliant bipedal locomotion on torque sensor-less gear-driven humanoid. In *2023 IEEE-RAS 22nd International Conference on Humanoid Robots (Humanoids)*, pages 1–8, 2023.

[16] H.R. Maturana and F.J. Varela. *Autopoiesis and Cognition: The realization of the living*, volume 42. Springer Science & Business Media, 2012.

[17] O. Mohseni, A.M.N. Rashty, A. Seyfarth, K. Hosoda, and M.A. Sharbafi. Bioinspired legged robot design via blended physical and virtual impedance control. *Journal of Intelligent & Robotic Systems*, 105(1):1–15, 2022.

[18] R. Müller, D.F.B. Häufle, and R. Blickhan. Preparing the leg for ground contact in running: the contribution of feed-forward and visual feedback. *Journal of Experimental Biology*, 218(3):451–457, 2015.

[19] Q.-V. Nguyen and H.C. Park. Design and demonstration of a locust-like jumping mechanism for small-scale robots. *Journal of Bionic Engineering*, 9(3):271–281, 2012.

[20] K. Nishikawa, A.A. Biewener, P. Aerts, A.N. Ahn, H.J. Chiel, M.A. Daley, T.L. Daniel, R.J. Full, M.E. Hale, T.L. Hedrick, A.K. Lappin, T.R. Nichols, R.D. Quinn, R.A. Satterlie, and B. Szymik. Neuromechanics: an integrative approach for understanding motor control. *Integrative and Comparative Biology*, 47(1):16–54, 05 2007.

[21] ODRI. ODRI Github Repository. https://open-dynamic-robot-initiative.github.io/, 2020. Last accessed 25 March 2021.

[22] D. Polani. An informational perspective on how the embodiment can relieve cognitive burden. In *2011 IEEE Symposium on Artificial Life (ALIFE)*, pages 78–85. IEEE, 2011.

[23] J. Proctor and P. Holmes. Reflexes and preflexes: on the role of sensory feedback on rhythmic patterns in insect locomotion. *Biological cybernetics*, 102(6):513–531, 2010.

[24] E.A. Rückert and G. Neumann. Stochastic optimal control methods for investigating the power of morphological computation. *Artificial Life*, 19(1):115–131, 2013.

[25] A. Spröwitz, A. Tuleu, M. Vespignani, M. Ajallooeian, E. Badri, and A.J. Ijspeert. Towards dynamic trot gait locomotion: Design, control, and experiments with cheetah-cub, a compliant quadruped robot. *The International Journal of Robotics Research*, 32(8):932–950, 2013.

[26] R.S. Sutton and A.G. Barto. *Reinforcement learning: An introduction*. MIT press, 2018.

[27] H.Q. Vu, H. Hauser, D. Leach, and R. Pfeifer. A variable stiffness mechanism for improving energy efficiency of a planar single-legged hopping robot. In *2013 16th International Conference on Advanced Robotics (ICAR)*, pages 1–7, 2013.